Proceedings of Global Power and Propulsion Society
ISSN-Nr: 2504-4400
GPPS Hong Kong 2023
October 17-19, 2023
www.gpps.global

GPPS-TC-2023-0089

INVESTIGATION OF MODIFIED SWEEPING JET FILM COOLING ON TURBINE VANE

Kechen Wang
Shanghai Jiao Tong University
kcwang@sjtu.edu.cn
Shanghai, China

Xu Zhang
Shanghai Jiao Tong University
zx977301567@sjtu.edu.cn
Shanghai, China

Wenwu Zhou*
Shanghai Jiao Tong University
zhouww@sjtu.edu.cn
Shanghai, China

Xin Wen
Shanghai Jiao Tong University
wenxin84@sjtu.edu.cn
Shanghai, China

Di Peng
Shanghai Jiao Tong University
idgnep8651@sjtu.edu.cn
Shanghai, China

Yingzheng Liu
Shanghai Jiao Tong University
yzliu@sjtu.edu.cn
Shanghai, China

ABSTRACT

The sweeping Jet (SJ) demonstrates potential applications in film cooling, due to its self-excited sweeping motion. Experiments were carried out to evaluate the cooling performance of the modified SJ and 777-shaped hole. The Fast pressure-sensitive paint (Fast-PSP) technique was utilized to measure the adiabatic film cooling effectiveness distributions over the suction side of the VKI LS89 vane. Carbon dioxide, serving as the coolant, was discharged into one row of holes located on the suction side surface at blowing ratios ranging from M = 0.25 to 0.75. In addition, the film cooling effectiveness of the modified SJ and 777-shaped hole on the pressure side surface at M = 1.0 and 2.5 was measured. The results indicate that the SJ exhibits higher cooling effectiveness values than the 777-shaped hole at both the suction side and pressure side, particularly in the spanwise direction.

INTRODUCTION

As an essential external cooling technique, film cooling is widely used in the cooling of hot components in gas turbines. The basic principle is that the cooling gas is ejected through discrete film holes and adheres to high-temperature surface to form a thin film, which isolates the high-temperature gas and prevents it from being eroded or melted (Han, Dutta and Ekkad, 2000). Cooling configurations have a significant impact on the cooling performance, directly determining the outlet momentum of the coolant and its interaction with the mainstream. There are various types of cooling configurations, circular holes, as the traditional film cooling configuration, were first applied to the cooling of turbine blades. However, the cooling gas is easily separated from the wall. Later, scholars proposed fan-shaped holes, which are gradually applied to turbine blade cooling (Han, Dutta and Ekkad, 2000) (Thole, 2014). For example, one of the widely used benchmark configurations, the 777-shaped hole, is obtained by expanding the circular hole in three directions along the streamline and spanwise by 7 degrees near the outlet. In recent years, with the development of advanced processing and manufacturing technologies, especially metal additive manufacturing, more novel cooling configurations, such as converging slot holes (Sargison *et al.*, 2002), sycee holes (Chang, Jing and Jiang, 2014), sister holes (Ely and Jubran, 2008), furcate holes (Liu *et al.*, 2021), and dune holes (Wang *et al.*, 2022), have been proposed. Though having achieved improvements in cooling performance, these configurations almost reach the bottleneck. Bunker (Bunker, 2010) has envisioned an unsteady film cooling method: the coolant exhibits periodic oscillation, and achieves uniform film coverage. However, this cooling method needs additional mechanical components to keep the oscillating motion.

The sweeping Jet (SJ) is a self-excited and oscillating flow. It has attracted widespread attention in the field of flow control (Wen *et al.*, 2020) (Wen, Liu and Tang, 2018). The SJ actuator mainly consists of an inlet, an outlet, a mixing chamber, a throat and a feedback channel. Its working process is that when the main jet enters the mixing chamber, the "Coanda" effect causes it to deflect and adhere to one side of the wall, and part of the fluid flows back through the feedback channel to produce reverse thrust. At the same time, the flow on the opposite side generates a large-scale separation bubble, which produces reverse thrust on the main jet. Under the dual effects of separation bubble and feedback flow, the jet changes trajectory and is directed towards the opposite wall, thus achieving periodic sweeping motion (Sieber *et al.*, 2016).

The periodic oscillating characteristics of SJ have attracted the attention of scholars in the field of film cooling. Kong et al. (Kong *et al.*, 2023) performed simulations to investigate the effect of different impinging distances for SJ cooling. They found that the cooling performance of SJ under different impinging distances is the same. Thurman et al. (Thurman *et al.*, 2016) and Hossain et al. (Hossain *et al.*, 2018) have applied SJ to flat plate film cooling. Their studies showed that compared to the 777-hole configuration, SJ can effectively enhance the cooling effectiveness value in the lateral direction at $M \geq 1.97$. Besides, they (Hossain *et al.*, 2019) employed the wake loss coefficient to assess the aerodynamic loss behavior of both the SJ and 777-shaped holes. The measurement of total pressure loss revealed a 12% rise in total pressure loss at $M = 1.5$ for the SJ, whereas the 777-shaped hole exhibited an 8% increase at the corresponding M. Furthermore, Hossain et al. (Hossain *et al.*, 2020) performed experimental and numerical investigations to study the SJ film cooling over the OSU vane by using infrared thermography. They found that the film coverage of SJ was more uniform than that of 777-hole, especially at $M \geq 2.0$. Sang et al. (Sang *et al.*, 2022) numerically studied the influence of coolant incident angle and exit fan angle on SJ flat plate film cooling. They concluded that reducing the SJ outlet width can increase its spanwise cooling effectiveness. Though the archived results showed the potential for the application of SJ on turbine blade cooling, existing SJ configurations are notably large. As a result, implementing such SJs in turbine blades can be challenging.

To address the challenge, Zhou et al. (Zhou *et al.*, 2022) devised a compact SJ. Fast pressure-sensitive paint (Fast-PSP) was utilized to measure the instantaneous cooling characteristics of compact SJ on a flat plate. They found that compared to the 777-shaped hole, the compact SJ can cover twice the spanwise area at high M, effectively improving film uniformity and reducing coolant consumption. However, the SJ design only showed improved cooling effectiveness at higher blowing ratios of $M > 2.5$, little benefit was observed in the relatively low M range. In this paper, the SJ geometry is modified with a shaped exit. Cooling effectiveness distributions of the modified SJ geometry over the suction side and pressure side of the VKI LS89 vane were measured using the Fast-PSP technique. Results indicate that the SJ exhibits higher cooling effectiveness values than the 777-shaped hole, particularly in the spanwise direction.

METHODOLOGY

Experimental setup and test model

Experiments were carried out in a single-passage transonic wind tunnel. The passage was designed based on the VKI LS89 turbine vane profile from Von Karman Institute (VKI), and the operating condition of MUR43 (Arts, Lambertderouvroit and Rutherford, 1990) was selected ($Ma_{exit} = 0.84$). The geometric information and the pressure taps on the vane surface can be found in the previous work of Qenawy et al. (Qenawy *et al.*, 2020). As shown in Fig. 1, a 132kW high-power air compressor provides the mainstream flow for the single-passage vane test rig. The mainstream flow passes through particle filters, oil filters, and water filters to ensure the dryness and cleanliness of the flow. The filtered air is then controlled by a pressure-reducing valve (SMC-AR925) at the inlet pressure. After entering a large collection chamber with a honeycomb layer, the mainstream flow is divided into three streams, each passing through the suction side (SS) bleed outlet, the pressure side (PS) bleed outlet, and the passage outlet, respectively. Flowmeters (SMC-PF3A706H) and valves are installed in each flow path to control the flow rate. Pressure sensors and K-type thermocouples are installed in the collection chamber to measure the total pressure and temperature of the mainstream flow, respectively. The secondary flow is provided by a high-pressure gas cylinder containing CO_2 (density ratio = 1.5) as the coolant source. The flow rate of coolant was monitored by a high-accuracy Omega flowmeter. The M ($\rho_c U_c$ / $\rho_\infty U_\infty$) was set to 0.25, 0.38, 0.50 and 0.75. The mass flow rate ratios (MFR) of SJ and 777-shaped hole corresponding to different M are as follows: for SJ, MFR = 2.2%, 3.4%, 4.5%, and 6.8%; for 777-shaped holes, MFR = 1.9%, 2.8%, 3.7%, and 5.5%. The temperature of the secondary gas was kept consistent with that of the mainstream flow by a water bath heating method.

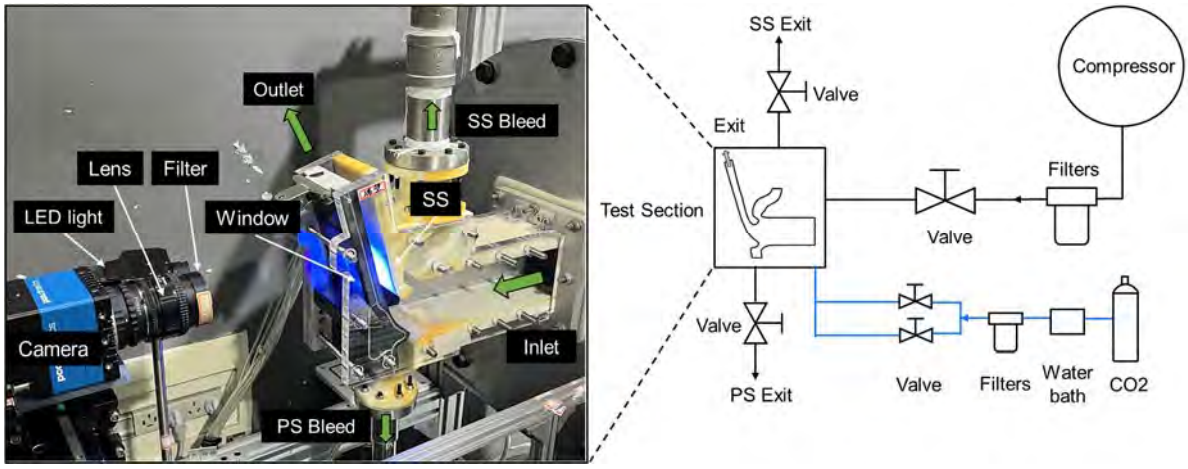

Figure 1 Suction Side Test Model Equipped with 777-shaped Hole and SJ.

The suction side test model is shown in Fig. 2, which displays the geometries of the 777-shaped hole and SJ configurations. The diameter D of film holes is 1.5 mm, and the spacing between holes is 6D. Six holes were arranged at the location of s/C = 0.27 on the suction side, and they were supplied with coolant from the same plenum. All holes had a hole inclination angle of 45°. Eight pressure taps were distributed on the surface for periodic validation. The baseline model utilized 777-shaped holes (Thole, 2014) with an exit width of 2.0D and a hole entry length of 5.2D (circular tube diameter is 1D). The modified SJ was designed based on the previous study (Zhou *et al.*, 2022), with the outlet deviating 7 degrees in both the spanwise and streamwise directions. The specific geometries of the SJ are as follows: the throat size is 0.8D × 1.3D, the hole exit size is 2.2D × 3.6D, the hole inlet size is 0.8D × 0.8D, the actuator width is 4.0D, and the exit angle is 60°. Both the 777 and SJ models were manufactured using resin 3D printing, with wax support used to ensure the smoothness and machining accuracy of the inner channels.

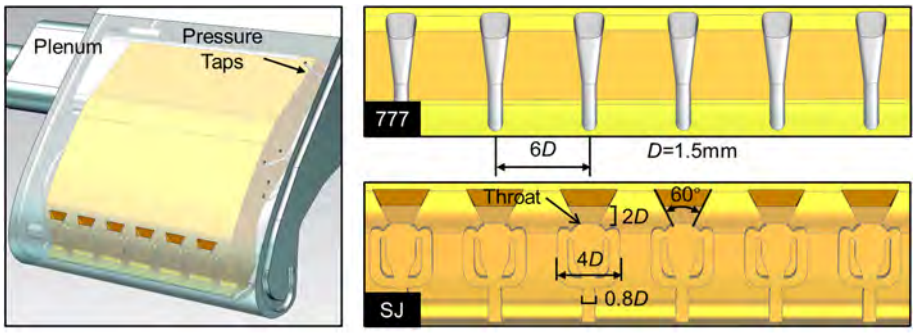

Figure 2 Suction Side Test Model Equipped with 777-shaped Hole and SJ.

The experimental setup for cooling effectiveness measurement on the pressure side is shown in Fig. 3. Due to the narrow channel of the vane, an endoscope (Wang *et al.*, 2022) was used to enter the upper side of the test section and capture the PSP signal on the pressure surface through a quartz glass (30×60 mm^2). The optical field is shown in the white region in Fig. 3. A 35mm focal length camera lens was mounted in front of the PCO 1600 camera (5 Hz). There were six SJs arranged on the pressure side of the vane with the same geometries as those on the suction side, while the hole inclination angle is 35°. The blowing ratios were set to 1.0 and 2.5. The *MFR* of SJ and 777-shaped hole corresponding to different M are as follows: for SJ, *MFR* = 3.4% and 5.7%; for 777-shaped holes, *MFR* = 2.8%, 3.7%, and 4.6%.

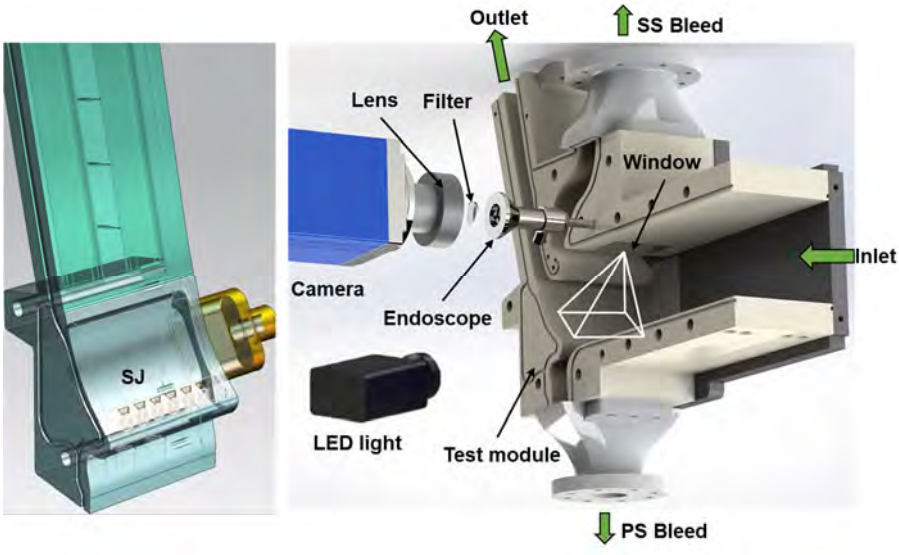

Figure 3 Pressure Side Test Model Equipped with 777-shaped Hole and SJ.

The isentropic Mach number (Ma_{is}) distribution can be calculated based on the static pressure distribution, as shown in Eq. (1).

$$Ma_{is} = \sqrt{\frac{2}{\gamma - 1}\left(\left(\frac{P_0}{P}\right)^{\frac{\gamma-1}{\gamma}} - 1\right)} \tag{1}$$

where P_0 is the stagnation pressure, P is the local static pressure, and γ represents the adiabatic index. The locations of the pressure tap that connected to the pressure scanning device (DAQ-DBX-32C) were based on VKI LS89. By adjusting the flow rate of the pressure bleed and suction bleed outlets, the Ma_{is} distribution over the vane surface can match the periodic distribution of the VKI results (Arts, Lambertderouvroit and Rutherford, 1990), thus satisfying the periodic conditions of the cascade. Figure 4 illustrates the periodic validation.

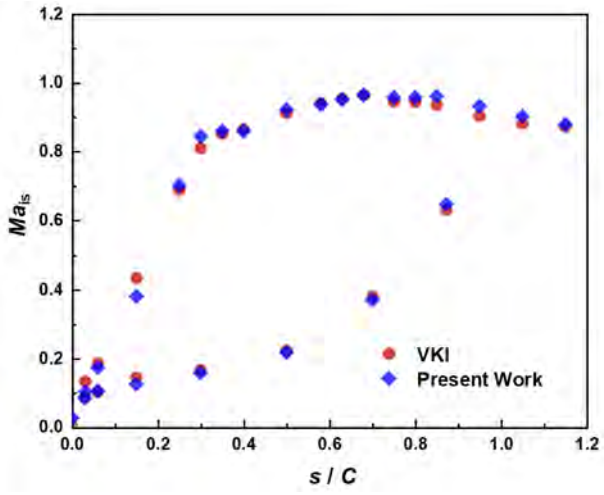

Figure 4 Periodic Validation of the Transonic Wind Tunnel.

PSP Technique

The cooling performance can be evaluated using a non-dimensional temperature parameter called adiabatic cooling effectiveness (η_{aw}), defined as Eq. (2):

$$\eta_{\mathrm{aw}} = \frac{T_\infty - T_{\mathrm{aw}}}{T_\infty - T_{\mathrm{c}}} \tag{2}$$

Here, T_{aw} represents the adiabatic surface temperature, while T_c and T_∞ represent the coolant jet and mainstream temperature, respectively. According to the heat-mass-transfer analogy theory of Jones (Jones, 1999) and Wright (Wright *et al.*, 2005), the η_{aw} can be expressed by oxygen concentration. During the experiment, secondary gases are discharged into the mainstream through film holes, with air being the typical incoming flow and oxygen-free gas such as CO_2 being used as the coolant jet. The oxygen-free gas can reduce the oxygen partial pressure at the wall. According to the work of Charbonnier et al., the expression for adiabatic cooling effectiveness for coolant with different density ratios (MW) is given by Eq. (3) (Charbonnier *et al.*, 2009). The P_{O2} represents the partial oxygen pressure.

$$\eta_{\mathrm{aw}} = 1 - \frac{P_{\mathrm{O2,coolant}}}{P_{\mathrm{O2,mainstream}}} = 1 - \frac{1}{\left[\left(P_{\mathrm{O2,air}}/P_{\mathrm{O2,wall}}\right) - 1\right]MW + 1} \tag{3}$$

The Fast-PSP technique (respond time < 50 μs) allows for quantitative measurement of oxygen partial pressure. This technique utilizes a fast-response coating of luminescent molecules (PtTFPP) that are sprayed onto the test surface. The luminescent molecules contain porous media and silica particles, which enable rapid diffusion of oxygen molecules in the coating. Once excited by an ultraviolet light (~400 nm), the luminescent molecules emit photoluminescence. By calibrating the relationship between the oxygen partial pressure and PSP signal, the adiabatic cooling effectiveness can be calculated. Previous studies (Zhou and Hu, 2016, 2017) provide additional details on the Fast-PSP and its calibration. Figure 1 illustrates the experimental setup, which involves the use of an ultraviolet LED (UHPT-LED-385) as the excitation source and a high-speed camera (PCO-HS4) for capturing emitted optical signals. To eliminate noise, a bandpass filter (650 ± 25 nm) was applied, and the sampling frequency was set to 4250 Hz. The experiment was conducted at an ambient temperature of 18 ± 0.5℃, and the main sources of uncertainty were attributed to image quality, PSP calibration, and equipment measurement error. Based on the error calculation study of PSP film cooling effectiveness measurement (Johnson and Hu, 2016), it was found that the absolute error of the film cooling effectiveness was $\Delta\eta$ = 0.014. Additionally, the relative uncertainty is approximately 1.6% for η = 0.60 and 4.9% for η = 0.25.

RESULTS AND DISCUSSIONS

Suction Side

Figure 4-5 shows the ensemble-averaged cooling effectiveness distribution on the suction side at M = 0.25, 0.38, 0.50 and 0.75. The calculation of ensemble-averaged cooling effectiveness was calculated by time-averaging the transient results, i.e., $\bar{\eta}(s,y)$, as shown in Eq. (4).

$$\bar{\eta}(s,z) = \frac{1}{t}\int_0^t \eta(s,z,t)dt \tag{4}$$

Figure 5 illustrates that at M = 0.25, the cooling effectiveness of SJ is noticeably higher than that of the 777-shaped hole, both in the spanwise and streamwise directions. The film of one single SJ primarily covers a spanwise area of approximately 6D, whereas that of the 777-shaped hole only covers 2D in the spanwise direction. Furthermore, the streamwise well-covered region (η > 0.4) of SJ extends up to s/D = 24, while that of the 777-shaped hole only extends to s/D = 10. Thus, under such M, the SJ has advantages over the 777-shaped hole in both spanwise and streamwise directions. When M increases to 0.38, the cooling performance of both 777 and SJ configurations in the streamwise direction is significantly improved. As shown in Fig. 6, when M further increases to 0.50, there is no significant improvement in the cooling performance of the SJ, while the streamwise cooling performance of the 777-shaped hole is further improved. Finally, when M increases to 0.75, the cooling effectiveness of both configurations decreases in the spanwise direction. This can be attributed to that the film is more likely to lift off from the surface at higher M. Compared to the 777-shaped hole, the streamwise film-coverage area of the SJ is slightly reduced, which is attributed to the partial use of coolant jet for streamwise oscillation dissipation. However, the high-effectiveness region of SJ can still maintain coverage up to 5D in the spanwise direction.

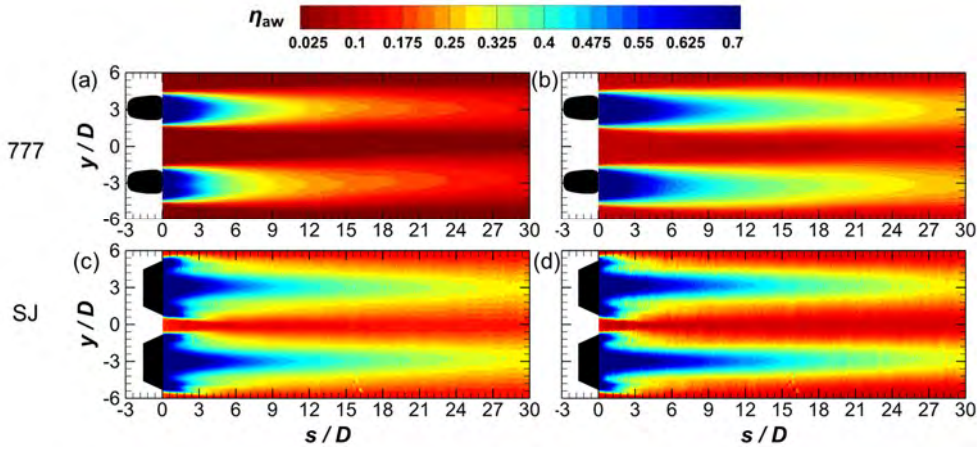

Figure 5 SS Effectiveness Distributions of 777-shaped Hole and SJ at *M* of 0.25 (a,c) and 0.38 (b,d).

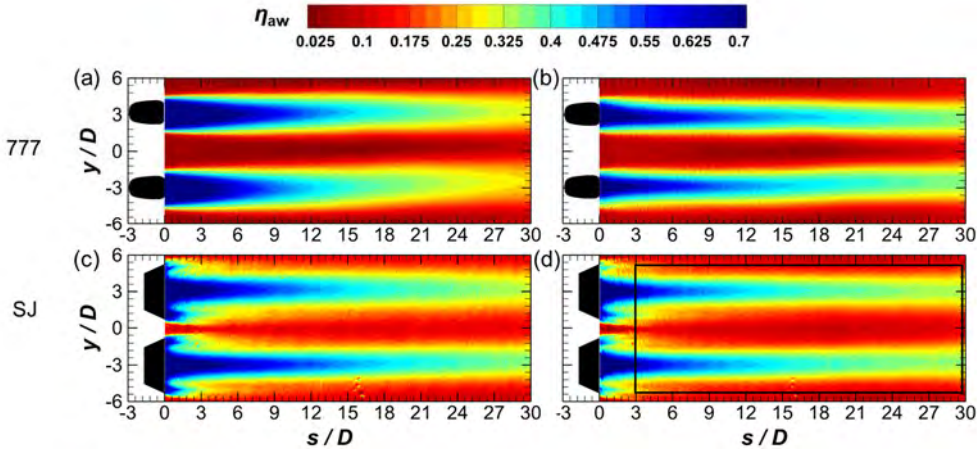

Figure 6 SS Effectiveness Distribution of 777-shaped Hole and SJ at *M* of 0.50 (a,c) and 0.75 (b,d).

Figure 7 shows the area-averaged effectiveness results. The integration was carried out within the area of $3 \leqslant s/D \leqslant 30$ and $-5 \leqslant y/D \leqslant 5$. According to the results, the SJ exhibits higher cooling effectiveness than the 777 configuration at all M,

particularly at M = 0.25, with an effectiveness value approximately 99.2% higher than that of the 777-shaped hole. However, the advantage of SJ over the 777-shaped hole gradually decreases with the increase of M, and finally, at M = 0.75, its film cooling effectiveness only improves by 6.73%.

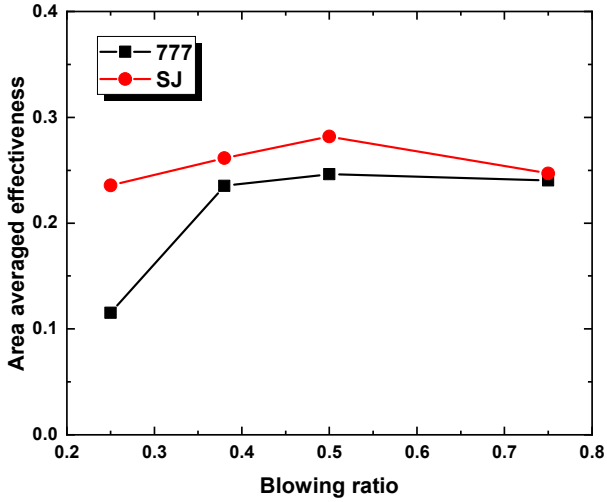

Figure 7 SS Area-Averaged Cooling Effectiveness of 777-shaped Hole and SJ.

Pressure Side

The ensemble-averaged effectiveness distributions of the 777-shaped hole and SJ at M = 1.0 and 2.5 are shown in Fig. 8. Results show that SJ performs significantly better on the PS than on the SS of the vane. When M = 1.0, the spanwise effectiveness of SJ far exceeds that of the 777-shaped hole, and its well-covered region (η > 0.3) can extend downstream to s/D = -15. When M is further increased to 2.5, the film of the 777-shaped hole exhibits obvious separation and reattachment, and its spanwise and streamwise cooling effectiveness is significantly reduced. However, SJ shows better performance at M = 2.5, presenting a rectangular film distribution in the -5<s/D<0 regions. This can be attributed to SJ's oscillation characteristics, where the sweeping motion consumes some of the jet momentum penetrating the mainstream, allowing SJ to better adhere to the wall surface under such high blowing ratios.

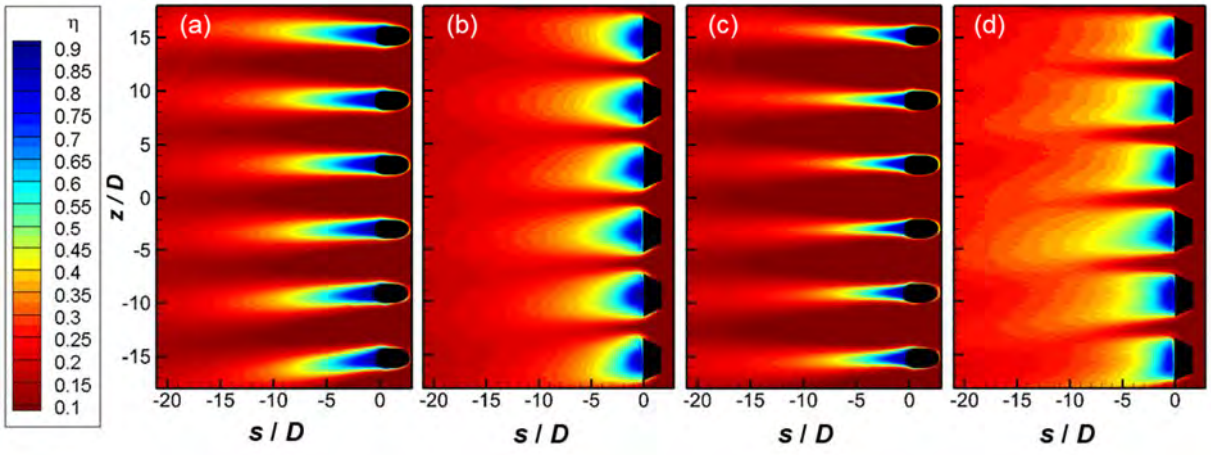

Figure 8 PS Effectiveness Distribution of 777-shaped Hole and SJ at *M* of 1.0 (a,b) and 2.5 (c,d).

The spanwise averaged cooling effectiveness was calculated using the data within the region of -18<z/D<18. According to Fig. 9, the SJ exhibits better cooling performance compared to the 777-shaped hole at both M = 1.0 and 2.5. When M=1.0, the advantage in film cooling of SJ is mainly reflected in the region of -5<s/D<0, and the cooling effectiveness value is improved by 60% compared to the 777 configuration. The cooling effectiveness of two configurations tends to be consistent in the downstream direction. However, when M increases to 2.5, SJ shows a huge advantage over the entire test surface. Compared with the 777 configuration, the SJ exhibits twice spanwise averaged effectiveness within the region of -5<s/D<-10.

The main reason for the observed differences in cooling performance between the SJ on the suction side and pressure side lies in the higher mainstream gas velocity on the suction side, where the separation is less favorable for the 777-shaped hole under low blowing ratios. Therefore, as the M increases, the advantage of the SJ over the 777-shaped hole gradually

diminishes at M<1.0 on the suction side. On the pressure side, where the mainstream gas velocity is lower near the surface, the 777-shaped hole gradually separates as M>1.0, while the SJ adheres well to the wall and sweeps along the spanwise direction, increasing the coverage area of the film. Consequently, on the pressure side, with increasing M, the advantage of the SJ over the 777-shaped hole becomes more pronounced. Considering the flow characteristics, the advantage of the SJ over the 777-shaped hole lies in its utilization of a portion of the jet momentum perpendicular to the surface for spanwise spreading. This not only enhances the spanwise coverage of the film cooling but also reduces the penetration of the SJ jet through the mainstream flow. As a result, the SJ is less prone to detachment from the surface, particularly at high M.

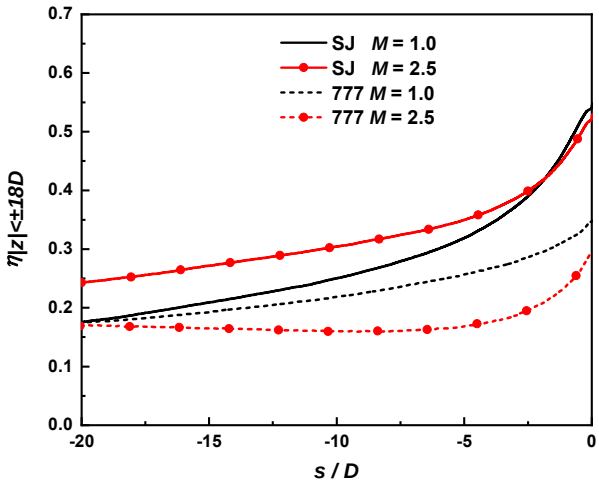

Figure 9 PS Spanwise Averaged Effectiveness of 777-shaped Hole and SJ.

CONCLUSIONS

In this paper, cooling effectiveness distributions of the 777-shaped hole and modified SJ were measured and analyzed using the Fast-PSP technique. Results reveal that the cooling effectiveness of the SJ is significantly superior to that of the 777-shaped hole. When the SJ is placed on the suction side, its cooling effectiveness values are significantly higher at low M (M = 0.25) than at higher M. When the SJ is placed on the pressure side, its cooling performance is significantly improved compared to the suction side, and with the increase of M, the cooling performance has a significant improvement in both spanwise and streamwise directions. The cooling effectiveness of SJ is approximately 105% higher than that of the 777-shaped hole. The obtained cooling effectiveness results contribute to a better understanding of SJ film cooling.

NOMENCLATURE

Abbreviations

C	Blade chord length
D	Hole diameter
Ma	Mach number
M	Blowing ratio
MW	Weight ratio (coolant/mainstream)
MFR	Mass flow rate ratio
PS	Pressure side
SS	Suction side
s/C	Vane span length to chord length ratio
η	Film cooling effectiveness

Subscripts

aw	Adiabatic wall
c	Coolant jet
∞	Mainstream flow

ACKNOWLEDGMENTS

The authors greatly acknowledge the financial support provided by the National Natural Science Foundation of China (No. 52276033, 92052107) for this study.

REFERENCES

Arts, T., Lambertderouvroit, M. and Rutherford, A. (1990) 'Aero-thermal investigation of a highly loaded transonic linear turbine guide vane cascade. A test case for inviscid and viscous flow computations', *NASA STI/Recon Technical Report N*, 91, p. 23437.

Bunker, R. S. (2010) 'Film Cooling: Breaking the Limits of Diffusion Shaped Holes', *Heat Transfer Research*, 41(6), pp. 627–650.

Chang, H., Jing, R. and Jiang, H. (2014) 'Experimental Investigations of SYCEE Film Cooling Performance on a Plate and a Tested Vane of an F-Class Gas Turbine'.

Charbonnier, D. *et al.* (2009) 'Experimental and Numerical Study of the Thermal Performance of a Film Cooled Turbine Platform', in *Asme Turbo Expo 2009, Vol 3, Pts A And B*. ASME, pp. 1027–1038. doi: 10.1115/GT2009-60306.

Ely, M. J. and Jubran, B. A. (2008) 'A Numerical Study on Increasing Film Cooling Effectiveness Through the Use of Sister Holes', in *ASME Turbo Expo 2008: Power for Land, Sea and Air*. Berlin, Germany, pp. 341–350. doi: 10.1115/GT2008-50366.

Han, J.-C., Dutta, S. and Ekkad, S. (2000) 'Gas Turbine Heat Transfer and Cooling Technology'.

Hossain, M. A. *et al.* (2018) 'Experimental and Numerical Investigation of Sweeping Jet Film Cooling', *Journal of Turbomachinery*, 140(3), p. 031009. doi: 10.1115/1.4038690.

Hossain, M. A. *et al.* (2019) 'Sweeping jet film cooling on a turbine vane', *Journal of Turbomachinery*, 141(3), pp. 1–11. doi: 10.1115/1.4042070.

Hossain, M. A. *et al.* (2020) 'Sweeping jet film cooling at high blowing ratio on a turbine vane', *Journal of Turbomachinery*, 142(12). doi: 10.1115/1.4047396.

Johnson, B. and Hu, H. (2016) 'Measurement uncertainty analysis in determining adiabatic film cooling effectiveness by using pressure sensitive paint technique', *Journal of Turbomachinery*, 138(12), pp. 1–11. doi: 10.1115/1.4033506.

Jones, T. V. (1999) 'Theory for the use of foreign gas in simulating film cooling', *International Journal of Heat and Fluid Flow*, 20(3), pp. 349–354. doi: 10.1016/S0142-727X(99)00017-X.

Kong, X. *et al.* (2023) 'Simulation on the effect of impinging distance for the aerodynamic and heat transfer characteristics of sweeping jet and film composite cooling', *Applied Thermal Engineering*, 227(July 2022), p. 120382. doi: 10.1016/j.applthermaleng.2023.120382.

Liu, C. L. *et al.* (2021) 'Film cooling performance evaluation of the furcate hole with cross-flow coolant injection: A comparative study', *International Journal of Heat and Mass Transfer*, 164, p. 120457.

Qenawy, M. *et al.* (2020) 'A Novel Single-Passage Transonic Wind-Tunnel for Turbine-Vane Film Cooling', *Journal of Engineering for Gas Turbines and Power*, 142(July), pp. 1–12. doi: 10.1115/1.4047284.

Sang *et al.* (2022) 'Numerical investigation of sweeping jet film cooling on a flat plate', *Thermal Science and Engineering Progress*, 29(September 2021), p. 101230. doi: 10.1016/j.tsep.2022.101230.

Sargison, J. E. *et al.* (2002) 'A Converging Slot-Hole Film-Cooling Geometry - Part 1: Low-Speed Flat-Plate Heat Transfer and Loss', *Journal of turbomachinery*, (3), p. 124.

Sieber, M. *et al.* (2016) 'Lagrangian coherent structures in the flow field of a fluidic oscillator', *Phys. Rev. Fluids*.

Thole, R. P. S. and K. A. (2014) 'Adiabatic Effectiveness Measurements for A Baseline Shaped Film Cooling Hole', in *ASME Turbo Expo 2014: Turbine Technical Conference and Exposition*. Düsseldorf, Germany, pp. 1–13. doi: 10.1115/GT2014-25992.

Thurman, D. *et al.* (2016) 'Investigation of spiral and sweeping holes', *Journal of Turbomachinery*, 138(9), p. 091007. doi: 10.1115/1.4032839.

Wang, K. *et al.* (2022) 'Transonic vane film cooling with crescent-shaped craters using an endoscopic pressure-sensitive paint technique', *Applied Thermal Engineering*, 205(September 2021), p. 118081. doi: 10.1016/j.applthermaleng.2022.118081.

Wen, X. *et al.* (2020) 'Flow dynamics of a fluidic oscillator with internal geometry variations', *Physics of Fluids*, 32(7). doi: 10.1063/5.0012471.

Wen, X., Liu, Y. and Tang, H. (2018) 'Unsteady behavior of a sweeping impinging jet: Time-resolved particle image velocimetry measurements', *Experimental Thermal and Fluid Science*, 96, pp. 111–127. doi: 10.1016/J.EXPTHERMFLUSCI.2018.02.033.

Wright, L. M. *et al.* (2005) 'Assessment of Steady State PSP, TSP, and IR Measurement Techniques for Flat Plate Film Cooling', in *Proceedings of ASME Summer Heat Transfer Conference 2005*. San Francisco, California, USA, pp. 1–10.

Zhou, W. *et al.* (2022) 'Spatiotemporal distributions of sweeping jet film cooling with a compact geometry', *Physics of Fluids*, 34(2). doi: 10.1063/5.0079391.

Zhou, W. and Hu, H. (2016) 'Improvements of film cooling effectiveness by using Barchan dune shaped ramps', *International Journal of Heat and Mass Transfer*, 103(12), pp. 442–456. doi: 10.1016/j.ijheatmasstransfer.2016.07.066.

Zhou, W. and Hu, H. (2017) 'A novel sand-dune-inspired design for improved film cooling performance', *International Journal of Heat and Mass Transfer*, 110, pp. 908–920. doi: 10.1016/j.ijheatmasstransfer.2017.03.091.